PERGAMON

International Journal of Heat and Mass Transfer 44 (2001) 375–387

International Journal of HEAT and MASS TRANSFER

www.elsevier.com/locate/ijhmt

Melting in a side heated tall enclosure by a uniformly dissipating heat source

Debabrata Pal[a], Yogendra K. Joshi[b,*]

[a]*Motorola, Inc., 1475 W. Shure Drive, M/S M638, Arlington Heights, IL 60004, USA*
[b]*Department of Mechanical Engineering, University of Maryland, College Park, MD 20742, USA*

Received 10 December 1999; received in revised form 9 March 2000

Abstract

Melting of an organic phase change material (PCM) *n*-triacontane ($C_{30}H_{62}$) in a side heated tall enclosure of aspect ratio 10, by a uniformly dissipating heat source has been studied computationally and experimentally. While heat transfer data for melting in enclosures under isothermal wall boundary condition are available in the literature, other boundary conditions, such as constant heat flux often arise in applications of PCM for transient thermal management of electronics. An implicit enthalpy–porosity approach was utilized for computational modeling of the melting process. Experimental visualization of melt front locations was performed. Comparisons between experimental and computational heat transfer data and melt interface locations were good. Fluid flow and heat transfer characteristics during melting suggested that natural convection plays a dominant role during initial stages of melting. At later times, the strength of natural convection diminishes as melting is completed. Correlations of heat transfer rate and melt fraction with time were obtained. © 2000 Elsevier Science Ltd. All rights reserved.

1. Introduction

Solid to liquid phase change materials (PCMs) including organic paraffins, metallic alloys and inorganic salts undergo reversible phase transitions, and act as thermal capacitors. They have been employed in the past extensively for passive solar energy storage and spacecraft thermal control. As an emerging application area, these materials also provide an efficient method of transient thermal control of electronic equipment. Most electronic systems are subjected to a complex combination of internal and external transient thermal loads. Thermal energy during such events can be stored within the PCM by melting it, and subsequently rejected to the ambient over extended periods by reversing the phase change [1]. During this sequence, the temperatures of critical components can be maintained nearly uniform. Possible applications of thermal management of electronic systems using PCM include cooling of portable systems, outdoor telecommunications enclosures and processor chips employing transient power management features. Design and optimization of such cooling modules require heat transfer data based on realistic thermal boundary conditions encountered in electronic packaging.

Melting due to isothermal heating conditions has been extensively studied. Hale and Viskanta [2] performed an experimental and analytical study of melting of several PCMs such as stearic acid, sodium phosphate dodecahydrate, sodium sulfate decahydrate, and *n*-octadecane, cooled or heated

* Corresponding author. Tel.: +1-301-405-5428; fax: +1-301-314-9477.
E-mail address: yogi@eng.umd.edu (Y.K. Joshi).

0017-9310/01/$ - see front matter © 2000 Elsevier Science Ltd. All rights reserved.
PII: S0017-9310(00)00116-2

Nomenclature

A	coefficients of source terms in momentum equations for PCM
c, c_p	specific heat (J/kg K)
D	thickness of the PCM layer (m)
Fo	Fourier number
g	acceleration due to gravity (m/s^2)
H	height of the PCM layer (m)
h	enthalpy (J/kg)
ΔH	latent heat content (J/kg)
k	thermal conductivity (W/m K)
L	latent heat of fusion of PCM (J/kg K)
Nu	Nusselt number
Q	total heat dissipation from module (W)
Q^+	heat dissipation per unit volume (W/m^3)
Ra	Rayleigh number
Ste	Stefan number
S	source terms in x, y and z momentum equations
S_h	source term in energy equation
T	temperature (°C)
T_m	melting point of PCM (°C)
T_0	Ambient temperature (°C)
u, v, w	dimensional velocity in x, y and z direction (m/s)
xl	dimension of side heated enclosure in x direction
yl	dimension of side heated enclosure in y direction
zl	dimension of side heated enclosure in z direction

Greek symbols

α	thermal diffusivity (m^2/s)
β	coefficient of volumetric expansion (1/K)
ε	volume fraction of molten PCM
ε_c	maximum temperature residual
ν	kinematic diffusivity (m^2/s)
θ	dimensionless temperature

from above or below. A one-dimensional analysis was performed using an empirical correlation to account for the effect of natural convection. Ho and Viskanta [3] reported on melting of *n*-octadecane inside an enclosure, with an isothermal left wall, the other walls being insulated. They studied the evolution of the melt front and measured heat transfer coefficients on the heated wall. A correlation of melting rate was also developed for conduction dominated regime of melting only.

Heat dissipation from electronic components can be modeled in many applications as uniform heat flux from a surface, or uniform dissipation within a volume. These types of heating events result in non-isothermal boundary conditions. Zhang and Bejan [4] studied melting within a tall enclosure (height/width = 5) filled with paraffin, due to a constant heat flux boundary condition. The opposite enclosure wall was maintained at a uniform temperature. Experiments were performed to determine the heat transfer coefficients and melting rates for various power dissipations. Based on an analytical approach involving boundary layer theory, a steady state heat transfer correlation was developed, which was found to be in good agreement with measurements.

Zhang et al. [5] experimentally studied the melting of *n*-octadecane by three flush mounted heat discrete heat sources inside a rectangular enclosure (100 mm tall × 60 mm deep × 50 mm wide). The heaters were mounted on the left vertical wall, and all other surfaces were maintained adiabatic. They experimentally measured the solid–liquid interface position and reported strong influence of natural convection. They reported limited data on melt fractions and temperatures for approximately the first 30% of the PCM melting.

Often in electronic systems the enclosure walls are relatively insulating. If PCMs are used for transient thermal management of internal electronic components, it is more realistic to assume these walls to be adiabatic rather than at a uniform temperature in design calculations. Such conditions appear to receive only limited prior attention. In this work, we investigate the detailed transient transport characteristics of melting from a uniformly dissipating source in a tall cavity, with other walls adiabatic. The melting process for *n*-Triacontane is computationally simulated and the results are compared with experimental data. The governing equations for melting with natural convection are solved using the enthalpy method. This approach for modeling phase change treats the solid and liquid as a single domain and does not require the explicit tracking of interface [6].

2. Experimental configuration and procedure

The experimental cell (Fig. 1) was constructed with 5.7 mm thick Lexan polycarbonate. A two part epoxy (Weldon-40) was used to join the walls to form a leak-proof container. A thin (thickness = 0.1 mm) etched film electrical heater on a kapton substrate of size ap-

proximately 127 mm × 127 mm, with an aluminum backing sheet (thickness = 0.19 mm) was used to simulate the uniformly dissipating heat source. The heater was mounted on one inner wall with a thin layer of Omegabond 101 thermally conductive epoxy (thermal conductivity = 0.7 W/m K), to minimize the thermal contact resistance. The aluminum backing sheet of the heater was exposed to the PCM.

A total of 17 copper–constantan thermocouples of 0.13 mm diameter were used (Fig. 1). Thermocouples were placed in position using a combination of Omegabond 101 and 0.127 mm thick double sided 3M adhesive. Thermocouples 1–5 were mounted on the backing sheet surface exposed to the PCM. These thermocouples were placed 25.4 mm apart, along a vertical line through the middle plane of the cell. Thermocouples 6–10 were mounted on the inner Lexan wall opposite to the heated surface. Thermocouples 11–15 were placed behind the heater, along the vertical mid plane. Thermocouples 16 and 17 were placed on either side of the mid plane at a distance of 25.4 mm, to assess the symmetry in the heating. The test cell was enclosed inside a 76 mm thick styrofoam insulation, during the entire duration of each run, to reduce heat loss from the system.

The transient thermocouple signals were conditioned and multiplexed by a signal conditioning module (National Instruments SCXI 1100), and were fed to a

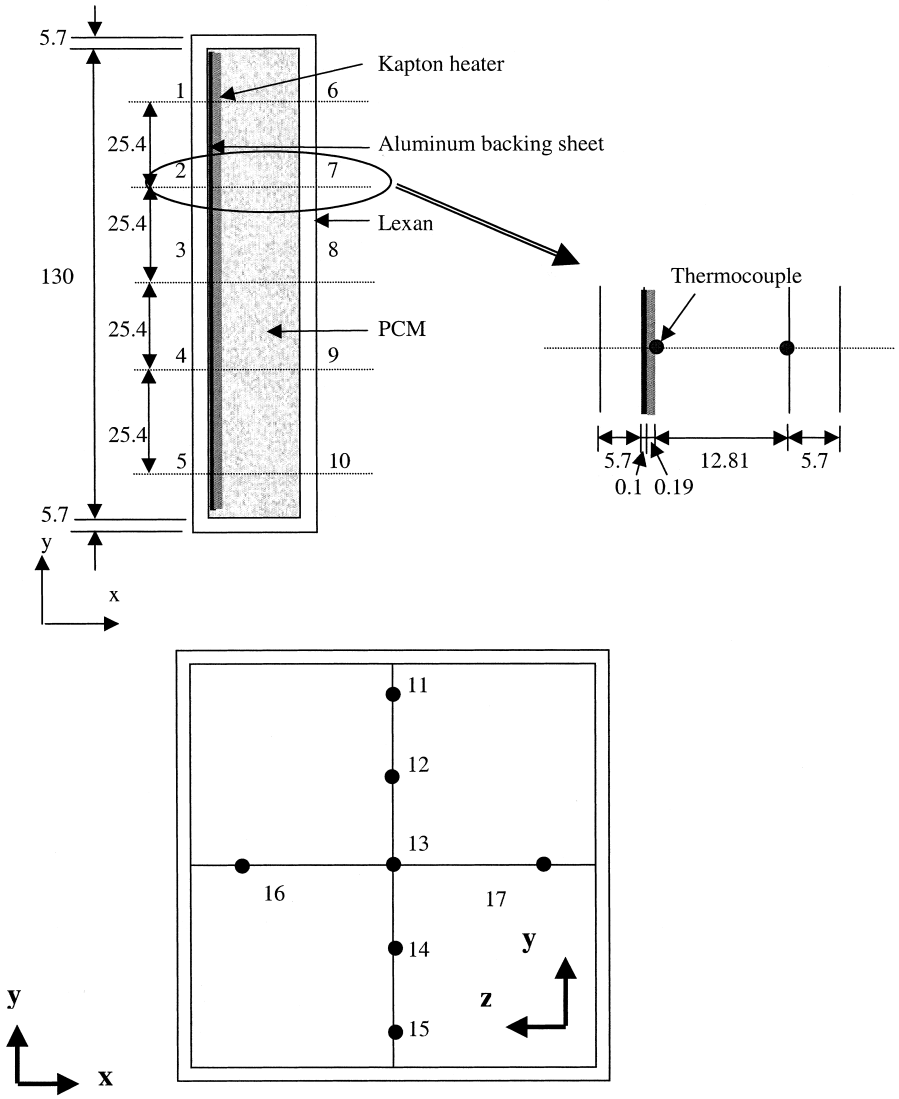

Fig. 1. Experiment cell (all dimensions are in mm).

data acquisition card (National Instruments AT-MIO-16-L-9). Power dissipation was determined by measuring current from the voltage drop across a known precision resistance, and voltage across the heat load. Commercial software (Labview) was used to acquire data from the thermocouples, and record them in a spreadsheet format on the computer, for further processing. The sampling rate for all experiments was 100 per second per channel, and 1000 samples per channel were averaged to record a single reading. Thus a time interval of 10 s was used for all data acquisition. The evolution of the solid–liquid interfaces was visualized using a high resolution video camera (SONY CCD Model SSC-C374). Selected video frames were digitized and later processed for determination of melt front shapes and propagation time measurements.

Before the experiments, the enclosure was slowly filled with molten PCM at a temperature of 95°C. The PCM was poured in 1 cm layers at a time, allowing the earlier layer to solidify, to ensure absence of any entrapped air bubble. Experiments were subsequently conducted with all the thermocouples initially uniform within ±0.15°C. Power to the heater was set and controlled by a variac. Experiments were continued until the maximum heater temperature rose to 105°C, the highest allowable operating temperature for the adhesives used in the setup. Tests were performed from 15 to 60 W at a step of 5 W. For each power level, at least three different runs were conducted to verify repeatability. All the transient temperatures recorded were found to be repeatable within ±2.5%.

An ice bath calibration of the electronic ice-junction based data acquisition card showed a consistent bias of 0.35°C against a precision mercury-in-glass thermometer (0.01°C resolution in the range of 0–100°C). This bias was corrected from the temperature measurements as part of the system calibration. An overall uncertainty of ±0.15°C was estimated in the temperature measurements. Uncertainties in mass and length measurements were ±0.1 g and ±0.5 mm, respectively. Uncertainties for voltage and current measurements were ±0.01 V and ±0.01 A, respectively. Individual uncertainties were combined in the constant odd form at 95% confidence level, using the technique by Kline and McClintock [7]. The resulting uncertainty for power measurement was ±0.3% for a power level of 60 W. The uncertainties for derived quantities were 0.6% for *Nu*, 4.9% for *Ra*, 4.0% for *Ste*, and 1% for θ.

3. Computational model

The fluid flow was assumed laminar due to the small velocities (~5 mm/s) encountered in the present study. Two-dimensional transport was considered, following experimental observations of the solid–liquid interface, which was uniform over a large region in the depthwise (z) direction. For all solids, the thermophysical properties were assumed to be independent of temperature. The density of molten PCM was assumed to be constant, except for the buoyancy force term in the y momentum equations, according to the Boussinesq approximation for natural convection flows. The time dependent conservation equations for mass, momentum and energy can be written as:

$$\text{Continuity:}\quad \frac{\partial u}{\partial x}+\frac{\partial v}{\partial y}=0 \tag{1}$$

x momentum:

$$\frac{\partial}{\partial t}(\rho u)+\frac{\partial}{\partial x}(\rho uu)+\frac{\partial}{\partial y}(\rho vu) = -\frac{\partial p}{\partial x}+\frac{\partial}{\partial x}\left(\mu\frac{\partial u}{\partial x}\right)+\frac{\partial}{\partial y}\left(\mu\frac{\partial u}{\partial y}\right)+S_x \tag{2}$$

y momentum:

$$\frac{\partial}{\partial t}(\rho v)+\frac{\partial}{\partial x}(\rho uv)+\frac{\partial}{\partial y}(\rho vv) = -\frac{\partial p}{\partial y}+\frac{\partial}{\partial x}\left(\mu\frac{\partial v}{\partial x}\right)+\frac{\partial}{\partial y}\left(\mu\frac{\partial v}{\partial y}\right)+S_y \tag{3}$$

Energy:

$$\frac{\partial}{\partial t}(\rho c_p T)+\frac{\partial}{\partial x}(\rho uc_p T)+\frac{\partial}{\partial y}(\rho vc_p T) = \frac{\partial}{\partial x}\left(k\frac{\partial T}{\partial x}\right)+\frac{\partial}{\partial y}\left(k\frac{\partial T}{\partial y}\right)+S_h \tag{4}$$

Eqs. (1)–(4) apply to the PCM and Eq. (5) (with $u=v=w=0$) applies to other solid materials. The expressions for coefficients and source terms for various materials in the above equations are listed in Table 1. The thermophysical properties of various materials are provided in Tables 2 and 3.

The source terms S_x, S_y, and S_z on the right-hand side of the momentum equations, are used to model the flow through the porous medium, near the solid–liquid interface [6]. C is a morphological constant, for a given material, and a value of 1.6×10^6 was chosen for the PCM, b is a small number $=1\times10^{-4}$, to prevent floating point overflow. For the simulation of melting of a pure metal, the melt front is a sharp line, and the existence of this porous medium ensures the gradual disappearance of the velocity field in the solid [6]. The calculation of the phase change interface was implicit, and was done *a posteriori*. At the dissimilar

Table 1
Source terms for various materials

	S_x	S_y	S_z	S_h
PCM	$\frac{C(1-\varepsilon)^2}{\varepsilon^3+b}u$	$\frac{C(1-\varepsilon)^2}{\varepsilon^3+b}v+\rho g\beta(T-T_m)$	$\frac{C(1-\varepsilon)^2}{\varepsilon^3+b}w$	$-\rho\frac{\partial(\Delta H)}{\partial t}$
Silicon	0	0	0	Q'''
Other solids	0	0	0	0

Table 2
Thermophysical properties used for computation

Materials	Thermal conductivity (W/m K)	Density (kg/m^2)	Specific heat (J/kg K)
Aluminum	204	2707	896
Adhesive (OB-101)	1	1150	1833
Lexan	0.19	1180	1255
Kapton	0.16	1200	1088

Table 3
Thermophysical properties of PCM used for computation

Material	Melting point (°C)	Latent heat (kJ/kg)	Density (kg/m^3)	Thermal conductivity (W/m K)	Specific heat (J/kg K)	Dynamic viscosity (kg m/s)
Gallium	29.78	80.16	6093	32	381.5	1.81×10^{-3}
n-Eicosene	37	241.0	790	0.23	2000	3.55×10^{-3}
n-Triacontane	65.4	251.0	810	0.23	2050	3.57×10^{-3}

material interfaces, heat balances were satisfied by using a harmonic mean formulation for thermal conductivities [8].

The code was validated by simulating melting of gallium in a two-dimensional cavity [6,9], of size $X = 8.89$ cm, and $Y = 6.35$ cm. Initially, the enclosure contained solid gallium slightly below its melting point, at $T_0 = 28.3$°C. At time $t = 0$, the left wall temperature was suddenly raised to $T_h = 38$°C. The right wall was maintained at $T_0 = 28.3$°C, and the top and bottom walls were insulated. The experimental and numerical data available in the literature in terms of melt front progression, were then compared with the present computational predictions. Following Brent et al. [6], a 42 × 32 uniform grid was used to discretize the domain. A time step of 5 s was used throughout the calculations. For the constant C in the momentum source terms, a value of 1.6×10^6 was used. For convergence, the maximum fractional change of temperature between two consecutive iterations (ε_c) was 1×10^{-6}. At the same time, the normalized energy balance residual (ε_c) was set as 1×10^{-4}. The results of computation are presented in Fig. 2. During the early stage of melting ($t = 2$ min), the interface was nearly planar due to conduction. With time, the effect of natural convection caused the interface shape to become oblique. Excellent agreement was observed with the existing computational and experimental results [6,9].

The computational domain for the current problem is shown in Fig. 1. The enclosure consisted of 5.7 mm thick Lexan plates. The vertical walls were spaced at 12.5 mm. The height of the enclosed space containing the PCM was 130 mm. The enclosure depth, or dimension normal to the plane was 130 mm, which was large enough to minimize the end effects on the melting rate, and fluid flow. An earlier study [10] focussed on the three-dimensional effects on melting inside a tall cavity. It was found that for an aspect ratio such as the one considered in the present study, the heat spreading through enclosure walls was negligible. The thermal conductivity of Lexan (0.19 W/m K) was close to that of the PCM (0.23 W/m K), which also reduced the three-dimensional conduction spreading effects near the boundaries. The heat source was 128 mm × 128 mm × 0.29 mm, with an aluminum backing sheet, and was modeled as a two-layer structure. The kapton layer was 0.1 mm thick, and was in contact with the inner left wall of the enclosure. On the other side of

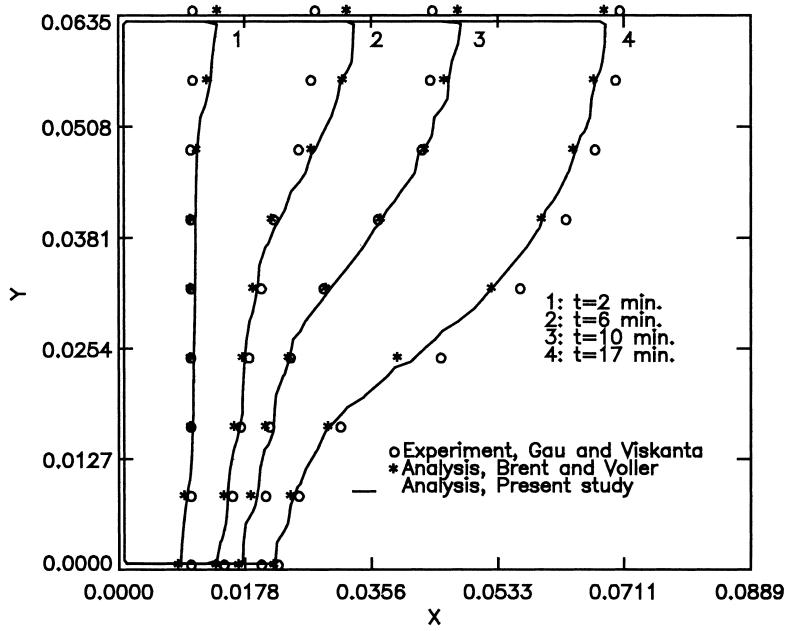

Fig. 2. Comparison of evolution of melt shapes.

the kapton layer was the 0.19 mm thick aluminum layer, which was exposed to the PCM. The heat source (kapton layer) was assumed to have constant thermophysical properties, and uniform volumetric heat dissipation. The computational domain in two-dimensions was discretized using a non-uniform 22×58 grid. A grid sensitivity study was done by using 17×46 and 27×60 grids. The results of this study are tabulated in Table 4. Based on these results for a power level of 30 W, the 22×58 grid was chosen for all computations. The last case in Table 2 with a three-dimensional $22 \times 58 \times 20$ grid confirms the adequacy of two-dimensional calculations for the configuration studied.

The thermal boundary conditions were:

$$x = 0, xl; \quad \frac{\partial T}{\partial x} = 0, \quad u = v = 0$$

$$y = 0, yl; \quad \frac{\partial T}{\partial y} = 0, \quad u = v = 0$$

4. Comparison between model predictions and experimental data

Fig. 3a compares the time-wise variations of temperature at various locations on the heater wall, for a power level of 15 W. Initially, the temperature increased rapidly with time, until the PCM began to melt. Following the initiation of melting, temperature of the heater was stabilized. This was followed by sensible heating of the liquid PCM and the other solids. The temperature variation along the heated wall was small during the pre-melt phase and the initial stage of

Table 4
Summary of grid sensitivity study

Grid size	Temperature (°C)	Percentage difference	Time to melt (s)	Percentage difference
17×46	91.50	−6.42	4140	6.15
22×58	97.78	0.00	3900	0.00
22×60	99.72	1.98	3820	−2.05
$22 \times 58 \times 20$	95.17	−2.67	3990	2.31

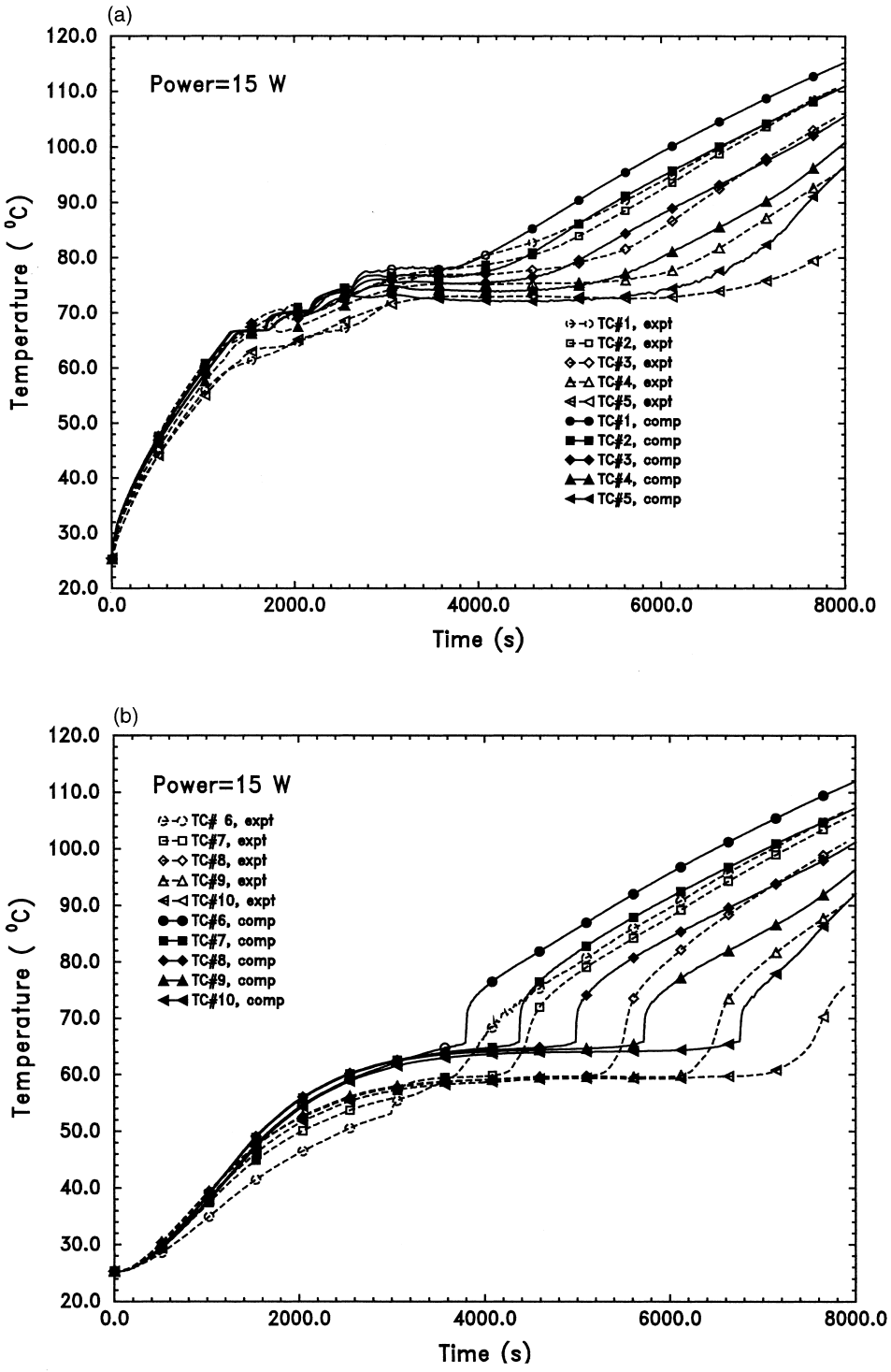

Fig. 3. Time-wise variation of temperature on the heated wall: (a) the right wall ($x = xl$), (b) for a power level of 15 W.

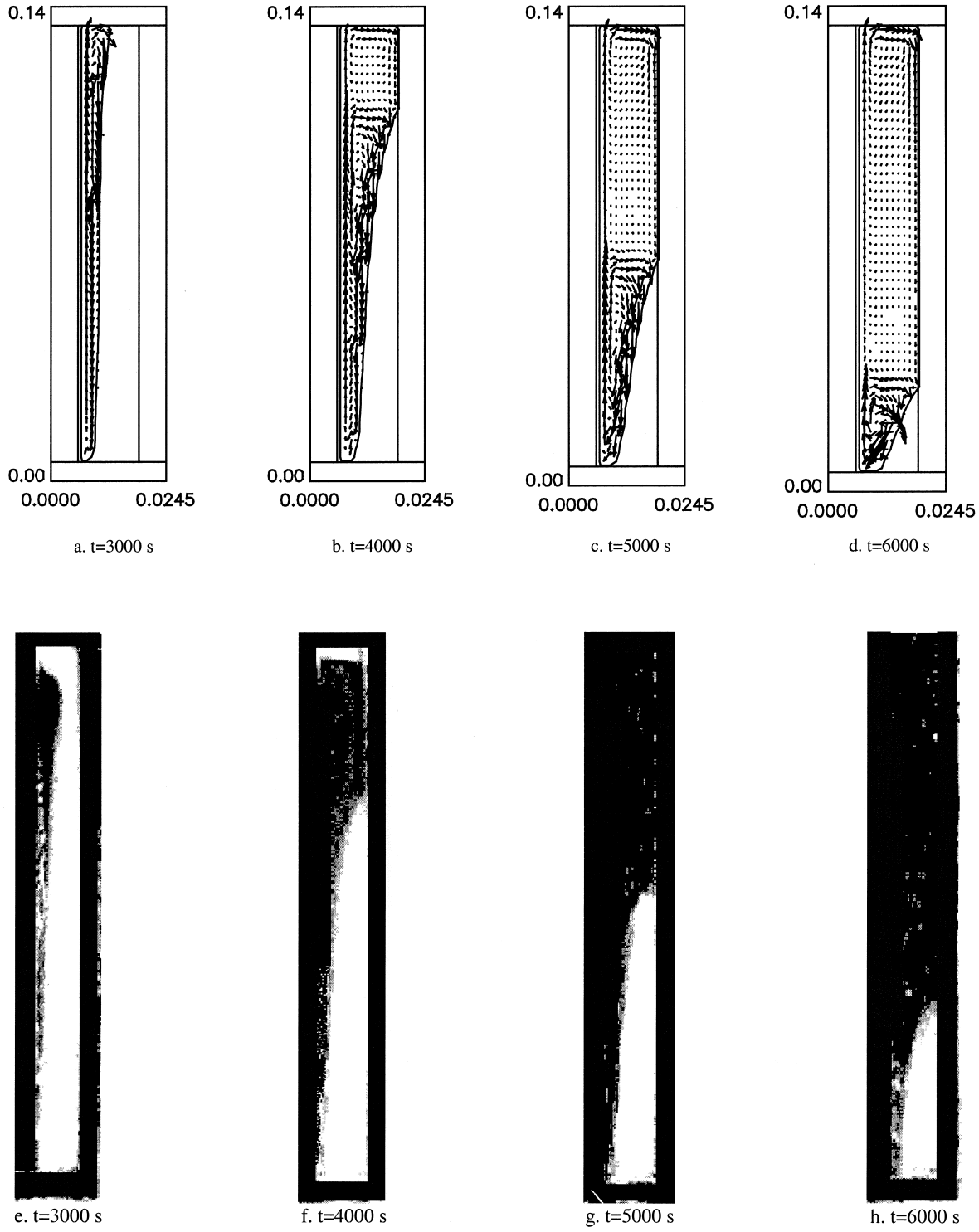

Fig. 4. Comparison between computed and experimental solid–liquid interfaces. The molten PCM appears to be dark and the solid PCM is seen as the white region.

melting, when the heat transfer was by conduction only. This caused the temperatures at various heights (TC 1–5), to fall within a narrow band. As the effects of convection became dominant, the temperature variation along the wall increased. The maximum measured and predicted temperatures of the heater were 100 and 105°C, respectively at $t = 7800$ s. The discrepancies between the computations and measurements can be attributed collectively to the variation of properties of various materials with temperature, non-isothermal melting of the PCM, and measurement uncertainties.

Fig. 3b shows the temperature variation on the right wall. The initial preheat was followed by temperature stabilization, and then a quick rise was observed in temperature at all thermocouple locations, in a sequence. This indicated the time of arrival of the solid/liquid interface at these points on the right wall. Since the melt interface was oblique (Fig. 4), the solid–liquid interface arrived first on the top (TC 6). This was followed by a downward progression, as the melt interface moved from TC 7 to TC 10.

5. Fluid flow and heat transfer characteristics

The computational results of evolution of melt front, and the velocity vectors are presented in Fig. 4a–d, for a power level of 15 W (heat flux = 0.093 W/cm^2). The corresponding experimental solid–liquid interface locations are visualized in Fig. 4e–h. As melting continues, buoyancy driven convection in the molten PCM starts to develop (Fig. 4a, e). During this stage, the hot and light molten PCM moves upward along the heated wall, turns around and moves towards the solid–liquid interface. This flow impinges on the solid–liquid interface, and transfers heat to the solid, which enhances melting.

Following the transfer of heat, the liquid PCM flows down along the solid–liquid interface. The effect of natural convection in the molten PCM causes a higher rate of melting near the top of the enclosure, and thus the melt shape becomes oblique, as heating continues. This observation of the transition from a conduction dominated melting to convection for the present boundary condition of uniformly dissipating heat source is similar to the melting inside an enclosure by an isothermal wall [3,11]. However, a boundary condition of uniform heat input on the wall caused some unique characteristics, which have not been studied before.

During the early stages of melting, the maximum velocity magnitude is small. It starts to increase as convection in the melt becomes dominant. For a power input of 15 W, the maximum velocity magnitude inside the molten PCM increased up to $t = 2400$ s. Follow-

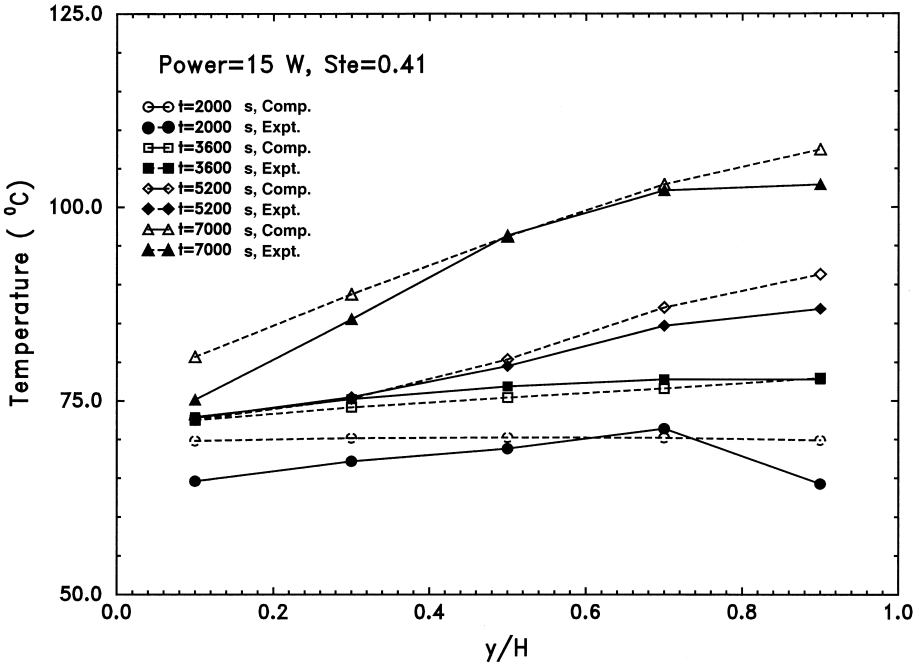

Fig. 5. Temperature variation on the heated wall for a power level of 15 W.

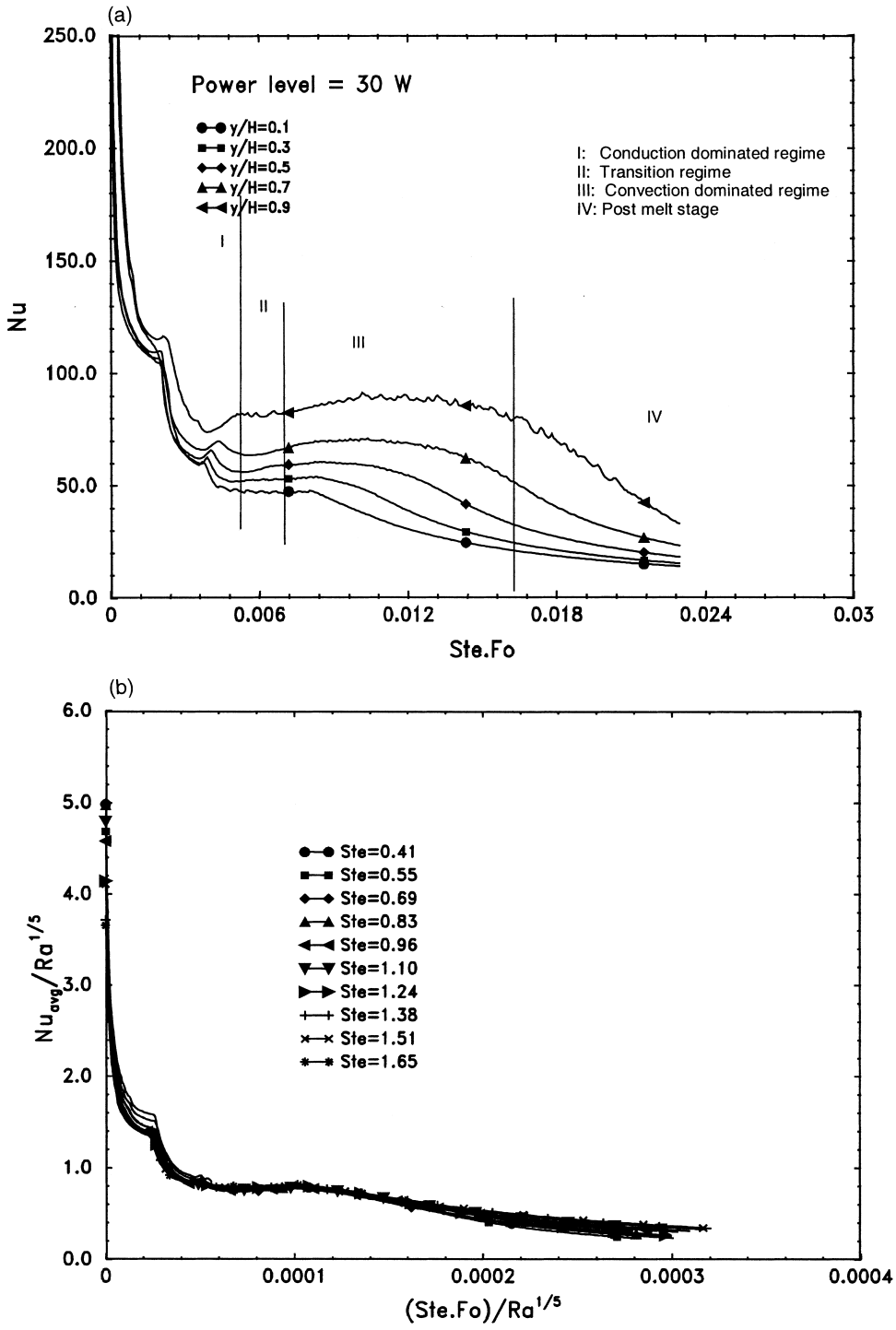

Fig. 6. Time-wise variation of local Nusselt number: (a) on the heated wall (computed) for a power level of 30 W, (b) average Nusselt number.

ing this time, the magnitude of velocity began to decrease with time. This was due to the fact that the walls were insulated, and the temperature in the molten PCM became more uniform with time, due to natural convection stirring. This caused a reduction in the buoyancy and a subsequent reduction in the velocity magnitude.

Spatial variation of temperature on the heated surface is presented in Fig. 5 at various times. During the early stages, temperature was more uniform along the heated wall due to the conduction dominated phase change. Due to the natural convection, the temperature variation on the heated wall became non-uniform with increasing values from bottom to top. This variation is important to consider in practical applications involving cooling of uniformly dissipating heat sources. The larger variations between the computations and the measurements near the ends are caused possibly due to larger conductive heat spreading effects near the heater edges.

6. Heat transfer and melting rates

The following non-dimensional parameters were used for normalizing the heat transfer results,

Fourier number, $Fo = \frac{\alpha(t-t_0)}{H^2}$, where t_0 is the time when melting begins

Stefan number, $Ste = \frac{c_p \Delta T}{L}$, where $\Delta T = \frac{QD}{kH^2}$

Rayleigh number, $Ra = \frac{g\beta QDH}{k\nu\alpha}$

Nusselt number, $Nu = \frac{Q}{kH(T-T_m)}$

Fig. 6a presents the time-wise variation of local instantaneous Nusselt number following melting at various locations on the heated wall for a power level of 30 W ($Ste = 0.81$). Starting with an infinite value at the initiation of melting Nusselt numbers drop very rapidly during the initial conduction dominated stage (I). This was followed by a sudden change in slope, which marked the beginning of a transition regime (II). During this phase, heat transfer was due to combined conduction and convection effects. Almost a constant value of Nu at a given location followed the transition stage. During the convection dominated stage of melting (III), Nu increased from the bottom to the top. As melting approached completion (IV), Nu started to reduce with time. This reduction was caused by sensible heating of the PCM, and lack of heat transfer from the system since all the boundaries were insulated. The difference in Nu along the heater began to reduce, as melting approached completion, indicating uniformity in temperature and a decreased strength of natural convection at this stage.

Determination of proper non-dimensional scales for melting and solidification processes is necessary to reduce the experimental and computational data in simpler forms. Difficulty in correlating heat transfer and melting rates, due to continuously changing length scales has been discussed by Beckermann [11] and Viskanta [12]. Various heat transfer and melting correlations have been attempted in the past [3,9,12–14] for isothermal wall boundaries. Zhang and Bejan [4] presented boundary layer analysis of side heated melting by constant heat flux surface. They analyzed the convection of molten PCM in the cold and the warm boundary layers, and then matched the solutions in the core region. The cold boundary layer refers to the layer at the solid–liquid interface and the warm boundary layer represents the layer next to the heated surface. In their analysis, the Nusselt number and dimensionless times were scaled with $Ra^{1/5}$.

For the present study, the thin heater can be assumed to be dissipating a nearly uniform heat flux, hence the scaling parameter of Zhang and Bejan [4] was used to reduce the heat transfer data. However, unlike in the study of Zhang and Bejan [4], where the right wall was kept at a constant temperature, the outer walls of the enclosure were kept thermally adiabatic in the present study to simulate compact electronic enclosures with relatively insulating walls. The average Nu on the heater wall were computed and displayed, normalized with $Ra^{1/5}$, as functions of scaled dimensionless time ($Ste \cdot Fo/Ra^{1/5}$) in Fig. 6b. Data for 10 different power levels reported collapsed on a single curve with the scaling of $Ra^{1/5}$. The various regimes of Nusselt number seen in Fig. 6b are similar to the ones described earlier in this section (Fig. 6a). The scaling of heat transfer data with $Ra^{1/5}$ showed larger difference in the collapsed data at times following melting, due to non-isothermal right wall.

Melt fractions were plotted against scaled dimensionless time ($Ste \cdot Fo/Ra^{1/5}$) in Fig. 7. The scaling collapses the data remarkably well. During the conduction and transition stage, the rate of melting showed a large variation, but reached an almost constant value during the convection dominated stage. At later stage, this rate started to drop with time, due to the decrease in natural convection.

Non-linear regression was used to fit the computed heat transfer results. The surface averaged Nu were correlated by the following equation,

$$\overline{Nu} = 0.01559\left[\frac{Ra^{1/5}}{Ste \cdot Fo}\right]^{0.4} \tag{5}$$

The molten volume fraction for all power levels were correlated by the following equation,

$$\varepsilon = 1.43\left(0.957 - e^{\frac{4865 Ste \cdot Fo}{Ra^{1/5}}}\right) \tag{6}$$

The range of validity of these two correlations is

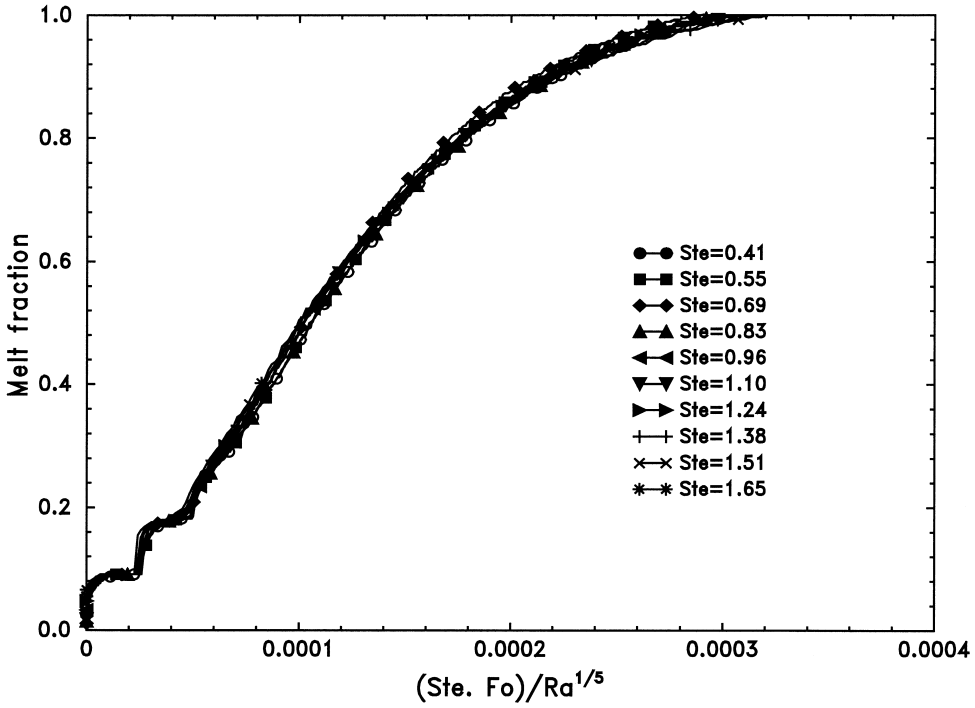

Fig. 7. Time-wise variation of melting rates (computed).

$[Ra^{1/5}/Ste \cdot Fo] < 0.0003$. These equations can be used to estimate the amount of PCM and the surface area required for thermal management of a uniformly dissipating heat source. These equations are only applicable to a side heated configuration. Effect of aspect ratio of the enclosure and non-adiabatic boundary conditions for all unheated surfaces have not been included. However, these equations should provide a conservative estimate in the early design phase of the cooling system.

7. Summary

Use of PCMs for various applications, where cooling is required for transient periods, is very promising due to its completory passive operation. This paper described an experimental and computational study of melting in a tall enclosure by a constant heat flux source and adiabatic boundaries, focussing attention on the effect of natural convection. The following conclusions can be drawn from the study:

1. For melting of PCM in a side-heated configuration the heat transfer was dominated by conduction during the early stages of melting. During the later stages, melting was affected significantly by natural convection. Following melting, the buoyancy induced flow was weakened due to reduced spatial thermal gradients, and sensible heat storage within the PCM caused its temperature to increase with time.
2. The shapes of the melt front obtained at various times from computations compared well with experiments.
3. The heat transfer data were scaled with $Ra^{1/5}$, following Zhang and Bejan [4]. This scaling reduced the normalized heat transfer and molten volume fraction data very well, except at the post-melt stage (Figs. 6b and 7). Differences at the post-melt stage are consistent with the fact that the right wall temperature started to increase following melting, due to sensible heating.
4. Good correlations for the volumetric molten fraction and heat transfer rates were obtained. Existing literature [4] had only considered constant temperature right wall, while applications such as electronics cooling often do not result in such well defined condition. The design correlations for heat transfer and molten fraction can be used to design a PCM filled heat sink for a given application where the heat source is vertically mounted.

References

[1] D. Pal, Y.K. Joshi, Application of phase change materials for passive thermal control of plastic quad flat packages (PQFP): a computational study, Numerical Heat Transfer. Part A 30 (1997) 19–34.

[2] N.W. Hale Jr., R. Viskanta, Solid–liquid phase-change heat transfer and interface motion in materials cooled or heated from above or below, Int. J. Heat and Mass Transfer 23 (1980) 283–292.

[3] C.J. Ho, R. Viskanta, Heat transfer during melting from an isothermal vertical wall, ASME Transations J. Heat Transfer 106 (February) (1984) 12–19.

[4] Z. Zhang, A. Bejan, Melting in an enclosure at constant rate, Int. J. Heat and Mass Transfer 32 (6) (1990) 1063–1076.

[5] Y. Zhang, Z. Chen, Q. Wang, Q. Wu, Melting in an enclosure with discrete heating at a constant rate, Experimental Fluid and Thermal Science 6 (1993) 196–201.

[6] A.D. Brent, V.R. Voller, K.J. Reid, Enthalpy–porosity technique for modeling convection–diffusion phase change: application to the melting of a pure metal, Numerical Heat Transfer 13 (1988) 297–318.

[7] S.J. Kline, F.A. McClintock, Describing uncertainties in single-sample experiments, Mechanical Engineering 75 (1953) 3–8.

[8] S. Patankar, Numerical Heat Transfer and Fluid Flow, Hemisphere, Washington, DC, 1980, pp. 44–45.

[9] C. Gau, R. Viskanta, Melting and solidification of a pure metal on a vertical wall, ASME Transactions J. Heat Transfer 108 (1986) 174–181.

[10] D. Pal, Y.K. Joshi, Computations of solid–liquid phase change in a three-dimensional enclosure by a uniformly dissipating heat source, in: Proceedings of the ASME National Heat Transfer Conference, Portland, Oregon, 1995, pp. 105–112.

[11] C. Beckermann, A general correlation for melting in rectangular enclosures, ASME Transactions J. Heat Transfer 111 (1989) 1111–1115.

[12] R. Viskanta, Natural convection in melting and solidification, in: S. Kakac, W. Aung, R. Viskanta (Eds.), Natural Convection: Fundamentals and Applications, Hemisphere, Washington, DC, 1985, pp. 845–877.

[13] C. Beckermann, R. Viskanta, Effect of solid subcooling on natural convection melting of a pure metal, ASME Transactions J. Heat Transfer 111 (1989) 416–424.

[14] C.J. Ho, C.H. Chu, The melting process of ice from a vertical wall with time-periodic temperature perturbation inside a rectangular enclosure, Int. J. Heat and Mass Transfer 36 (13) (1993) 3171–3186.